

An inertial and magnetic sensor based technique for joint angle measurement

Karol J. O'Donovan^{a,*}, Roman Kamnik^b, Derek T. O'Keefe^a, Gerard M. Lyons^a

^a*Biomedical Electronics Laboratory, Department of Electronic and Computer Engineering, University of Limerick, Limerick, Ireland*

^b*Laboratory of Robotics and Biomedical Engineering, Faculty of Electrical Engineering, University of Ljubljana, Ljubljana, Slovenija*

Accepted 20 December 2006

Abstract

This paper describes the design and evaluation of a miniature kinematic sensor based three dimensional (3D) joint angle measurement technique. The technique uses a combination of rate gyroscope, accelerometer and magnetometer sensor signals. The technique enables 3D inter-segment joint angle measurement and could be of benefit in a variety of applications which require monitoring of joint angles. The technique is not dependent on a fixed reference coordinate system and thus may be suitable for use in a dynamic system such as a moving vehicle. The technique was evaluated by applying it to joint angle measurement of the ankle joint. Experimental results show that accurate measurement of ankle joint angles is achieved by the technique during a variety of lower leg exercises including walking.

© 2007 Elsevier Ltd. All rights reserved.

Keywords: Joint angle measurement; Gyroscope; Accelerometer; Magnetometer

1. Introduction

Accurate three-dimensional (3D) inter-segment joint angle measurement is an important biomechanical measure for a variety of applications. Such a measure when applied to ankle joint measurement could be used for the monitoring of lower leg activity in persons with limited mobility that are at risk of remaining inactive for prolonged periods. It could also be used for the measure of balanced dorsiflexion (rotation about the medio-lateral axis of the joint which does not also involve rotation about the other axes of the joint) in drop foot correction applications or for the monitoring of foot rotation in clinical trials.

Various kinematic sensor techniques have been developed for the study of gait analysis (Mayagoitia et al., 2002; Veltink et al., 2003; Williamson and Andrews, 2001), monitoring upper extremity kinematics (Luinge and Veltink, 2005) and mobility monitoring (Lyons et al., 2005).

Joint angle and segment inclination measurement techniques have been developed for gait analysis which use accelerometers on their own (de Vries et al., 1994; Willemsen et al., 1990) or combined with rate gyroscopes (Luinge and Veltink, 2005; Mayagoitia et al., 2002; Williamson and Andrews, 2001). These techniques measure the inclination of a segment with respect to a common reference axis (the gravity vector) and hence determine a two-dimensional (2D) joint angle between two segments. The application of these techniques is limited in that joint angles can only be measured about a single axis (2D joint angle measurement) and this axis must be close to perpendicular to the gravity vector reference axis. The use of accelerometers on their own is also limited to quasi-static activity.

Three dimensional angle measurement requires the addition of a second reference axis. Veltink (Veltink et al., 2003) successfully developed a 3D technique for monitoring foot orientation during walking using the direction of progression as a second reference axis. However, this technique is limited to use during ambulation only. A number of 3D segment orientation measurement techniques have been developed which have incorporated

*Corresponding author. Tel.: +353 85 7209471; fax: +353 61 338176.
E-mail address: karol.odonovan@gmail.com (K.J. O'Donovan).

magnetic sensors to compliment kinematic sensors using the magnetic field vector as a second reference axis. These techniques allow absolute orientation measurement of the segment with respect to a common fixed reference coordinate system derived from the two fixed reference vectors. Kemp et al. (1998) assume that the only acceleration is the gravity vector and so the technique which they developed is only suitable for quasi-static applications while other studies have accounted for small changes in acceleration and magnetic field interference using Kalman filter equations (Bachmann, 2000; Foxlin, 1996; Roetenberg et al., 2005).

If a subject is contained within a moving vehicle such as a car or aeroplane the dynamics are such that the magnitude and direction of the measured acceleration vector may vary significantly with time. The measured magnetic field vector may also vary over time. Local magnetic interference may cause significant changes in the direction of the measured magnetic field vector. Also, the magnetic field angle of inclination (the angle of the earth's magnetic field vector with respect to the surface of the earth) is different at different locations around the world, having a value of 90° at the earth's magnetic poles and a value close to 0° near the equator (Rukstales and Quinn, 2001). The direction of the magnetic field vector, with respect to the earth's surface thus drifts as one travels in a north–south longitudinal direction and also to a lesser extent as one travels in an east–west latitudinal direction. A reference coordinate system which varies in time cannot be used to determine the absolute orientation of a segment.

The technique presented in this paper is concerned with joint angle measurement. Joint angles are determined from the orientation of one segment relative to another and are not concerned with absolute segment orientation. A complimentary inertial/magnetic sensor based technique is presented which can be used to measure 3D joint angles between two body segments. It is dependent only on the periodic existence of a common reference coordinate system which need not be fixed and may be suitable for use in a dynamic system.

2. Methods

2.1. Sensor design

Two acceleration, angular rate and magnetic (AARM) sensors are used in the technique, one attached to the foot segment and the other attached to the lower leg segment. Each AARM contains a tri-axial accelerometer, rate gyroscope, and magnetometer configuration. The tri-axial accelerometer is formed from the combination of two bi-axial Analog Devices ADXL210E accelerometers. Each ADXL210E is sensitive to both gravity induced static acceleration and movement induced dynamic acceleration and will measure accelerations with a full-scale range of $\pm 10g$. The tri-axial rate gyroscope consists of three uni-axial Analog Devices ADXRS150 rate gyroscopes. Each ADXRS150 was configured to measure angular rates up to 300°s^{-1} through the use of a single external resistor. The tri-axial magnetometer used is the Honeywell HMC2003 magnetic sensor. The HMC2003 is capable of sensing magnetic fields as low as $30 \mu\text{G}$.

2.2. Sensor calibration

The tri-axial accelerometer output signal \hat{y}_a is modelled as (Ferraris et al. 1995)

$$\hat{y}_a = K_a R_a \hat{a} + \hat{b}_a, \quad (1)$$

where \hat{a} is the 3×1 acceleration vector, \hat{b}_a the 3×1 accelerometer offset vector, K_a the 3×3 accelerometer sensitivity matrix and R_a the 3×3 accelerometer misalignment matrix.

Similarly the tri-axial rate gyroscope output signal \hat{y}_g is modelled as

$$\hat{y}_g = K_g R_g \hat{\omega} + \hat{b}_g, \quad (2)$$

where $\hat{\omega}$ is the 3×1 angular velocity vector, \hat{b}_g the 3×1 gyroscope offset vector, K_g the 3×3 gyroscope sensitivity matrix and R_g the 3×3 gyroscope misalignment matrix.

Constant values for K_a , R_a , K_g and R_g , and initial values for the accelerometer offset \hat{b}_a and gyroscope offset vector, \hat{b}_g , are calculated using the method calibration procedure outlined by Ferraris et al. (1995). The accelerometer offset is updated prior to use under static conditions using the technique described by Lötters et al. (1999). The rate gyroscope offset is re-calculated in-use during periods when rotational activity is static using Algorithm 1.

Algorithm 1.

If

$$\sqrt{\frac{1}{N} \sum_{k=N}^k \left(\hat{y}_{g(k)} - \left(\frac{1}{N} \sum_{k=N}^k \hat{y}_{g(k)} \right) \right)^2} \leq \hat{\sigma}$$

then

$$\hat{b}_g = \frac{1}{N} \sum_{k=N}^k \hat{y}_{g(k)},$$

where $\hat{y}_{g(k)}$ is the 3×1 output signal vector from the gyroscope at sample point k . The 3×1 threshold vector $\hat{\sigma}$ is calculated as the standard deviation vector when the gyroscope was held static for a period of 5 s during the initial calibration procedure. If low variance of the gyroscope signal on each axis is detected for a period of 2 s ($N = 2f_s$ samples, where f_s is the sensor sampling frequency), the offset of the rate gyroscope is re-calculated as the mean output signal during that period.

The magnetometer output signal \hat{y}_m is modelled as

$$\hat{y}_m = K_m R_m \hat{m} + \hat{b}_m, \quad (3)$$

where \hat{m} is the 3×1 magnetic field vector, \hat{b}_m the 3×1 magnetometer offset vector, K_m the 3×3 magnetometer sensitivity matrix, and R_m the 3×3 magnetometer misalignment matrix. These constants were calculated using a novel magnetometer calibration technique developed by the authors (a technical note describing the technique is currently under review).

2.3. Determining the ${}^{\text{SENI}}R_{\text{SEGi}}$ orientation matrix

Each sensor unit is attached securely to the respective segment such that the orientation of the sensor unit with respect to the body segment does not change. Typically the orientation of the sensor unit coordinate system will not be aligned with the chosen reference coordinate system of the body segment. An orientation matrix ${}^{\text{SENI}}R_{\text{SEGi}}$ is used to describe the orientation of the body segment coordinate system with respect to the coordinate system of the sensor unit attached to it, where 'i' is used as the index number for the body segment, the foot being indexed '1' and the leg being indexed '2'.

Once the sensor units are attached to the body segments, their respective orientation matrices, ${}^{\text{SENI}}R_{\text{SEGi}}$ and ${}^{\text{SENI}2}R_{\text{SEGi}2}$ are calculated using a novel two stage technique. Firstly with the subject standing upright as in Fig. 1(a), a rotation about the longitudinal axis of the whole body is performed. In theory the rotation can be of any angle greater than 0° and

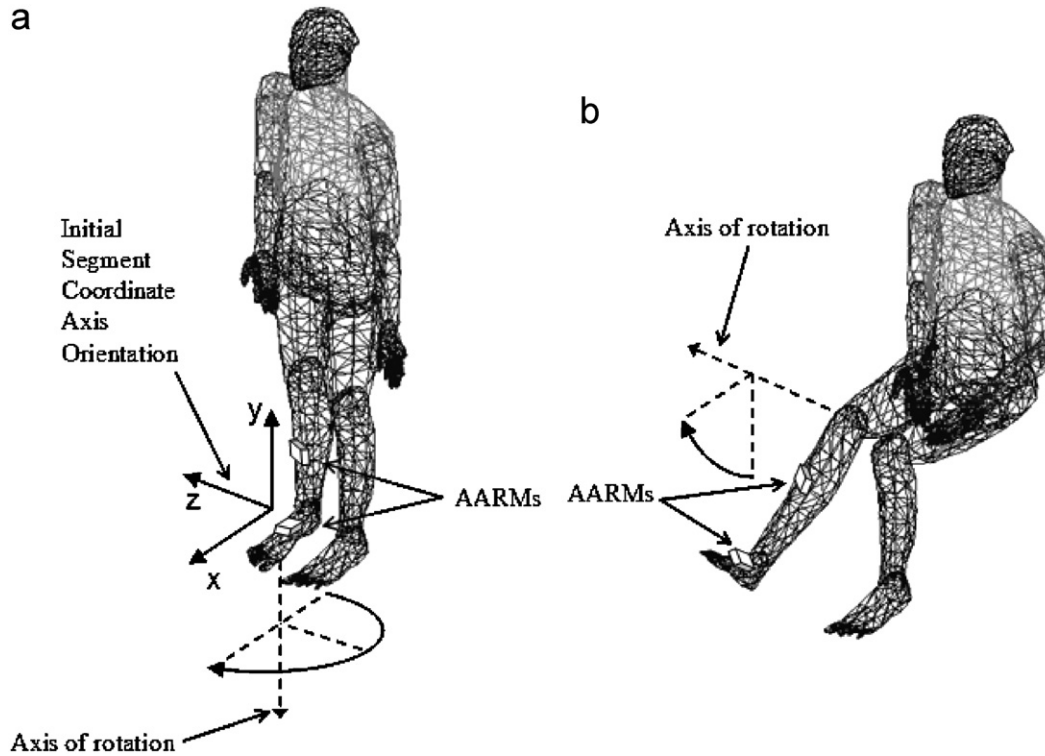


Fig. 1. (a) Procedure for the determination of the segment y -axis with respect to the sensor (AARM) coordinate system and (b) procedure for the determination of the segment z -axis with respect to the sensor (AARM) coordinate system.

less than 360° but an angle of 180° is used for optimal results. This rotation involves a rotation of both the foot and leg segments about their respective y -axes. The change in orientation and hence the axis of rotation can be determined from strapdown integration of the gyroscope signal. The axis of rotation corresponds to the y -axis of the segment with respect to the sensor coordinate system, ${}^{\text{SENI}}\hat{y}_{\text{SEGI}}$.

Secondly with the subject seated in the neutral position as in Fig. 1(b), and the foot positioned with respect to the leg so that the medio-lateral axes of both segments are aligned in parallel, a knee extension with minimal movement of the ankle joint is performed. This involves rotation of both the foot and leg about their respective z -axes. Strapdown integration of the gyroscope signals is again used to determine the axis of rotation and hence determine the z -axis of each segment with respect to the sensor coordinate system, ${}^{\text{SENI}}\hat{z}_{\text{SEGI}}$. The x -axis of each segment is determined as the cross product of the y -axis and z -axis.

The 3×3 orientation matrix ${}^{\text{SENI}}R_{\text{SEGI}}$ is then given by the set of three column vectors:

$${}^{\text{SENI}}R_{\text{SEGI}} = \begin{bmatrix} {}^{\text{SENI}}\hat{x}_{\text{SEGI}} & {}^{\text{SENI}}\hat{y}_{\text{SEGI}} & {}^{\text{SENI}}\hat{z}_{\text{SEGI}} \end{bmatrix}. \quad (4)$$

2.4. Determining the ${}^{\text{REF}(k)}R_{\text{SEGI}(k)}$ orientation matrix

An orientation matrix, ${}^{\text{REF}(k)}R_{\text{SENI}(k)}$, describing the orientation of each sensor unit with respect to common reference coordinate system at sample point k can be derived if at each instant there are two common reference vectors \hat{v}_1 and \hat{v}_2 which are measured equally by both sensor units and are in different directions.

The normalised common vector 1 can be chosen as the y -axis of the reference coordinate system:

$${}^{\text{SENI}(k)}\hat{y}_{\text{REF}(k)} = \frac{{}^{\text{SENI}(k)}\hat{v}_1(k)}{|{}^{\text{SENI}(k)}\hat{v}_1(k)|}. \quad (5)$$

The x -axis is calculated as the normalised cross product of common vector 2 and the y -axis:

$${}^{\text{SENI}(k)}\hat{x}_{\text{REF}(k)} = \frac{{}^{\text{SENI}(k)}\hat{v}_2(k) \times {}^{\text{SENI}(k)}\hat{y}_{\text{REF}(k)}}{|{}^{\text{SENI}(k)}\hat{v}_2(k) \times {}^{\text{SENI}(k)}\hat{y}_{\text{REF}(k)}|}. \quad (6)$$

Finally the z -axis is calculated as the cross product of the y -axis and the x -axis:

$${}^{\text{SENI}(k)}\hat{z}_{\text{REF}(k)} = {}^{\text{SENI}(k)}\hat{y}_{\text{REF}(k)} \times {}^{\text{SENI}(k)}\hat{x}_{\text{REF}(k)}. \quad (7)$$

The 3×3 orientation matrix ${}^{\text{SENI}(k)}R_{\text{REF}(k)}$ is then given by the set of three column vectors:

$${}^{\text{SENI}(k)}R_{\text{REF}(k)} = \begin{bmatrix} {}^{\text{SENI}(k)}\hat{x}_{\text{REF}(k)} & {}^{\text{SENI}(k)}\hat{y}_{\text{REF}(k)} & {}^{\text{SENI}(k)}\hat{z}_{\text{REF}(k)} \end{bmatrix}. \quad (8)$$

Using the derived orientation matrix ${}^{\text{SENI}(k)}R_{\text{REF}(k)}$, and the orientation matrix ${}^{\text{SENI}}R_{\text{SEGI}}$ derived in Section 2.3, an orientation matrix ${}^{\text{REF}(k)}R_{\text{SEGI}}$ which describes the orientation of each segment with respect to the common reference coordinate system can be derived:

$${}^{\text{REF}(k)}R_{\text{SEGI}(k)} = {}^{\text{SENI}(k)}R_{\text{REF}(k)}^{-1} {}^{\text{SENI}(k)}R_{\text{SEGI}(k)}. \quad (9)$$

2.5. Obtaining two common reference vectors

If we assume that the magnetic field in the vicinity of the foot is the same magnetic field in the vicinity of the leg then the magnetic field vector measured by each sensor unit is a different measurement of the same vector. The magnetic field vector can thus be used as common vector number one. Note that this assumption holds in cases where there is local magnetic interference as long as the magnetic interference is such that it does not cause discrepancies in the magnetic field at the foot and the

magnetic field at the leg.

$$\text{SENi}^{(k)} \hat{v}_{1(k)} = \text{SENi}^{(k)} \hat{m}. \quad (10)$$

The total acceleration of the segment, $\hat{a}_{T \text{ SEGi}}$, measured by an accelerometer, can be described as the sum of the acceleration vector due to linear movement of the segment, $\hat{a}_{L \text{ SEGi}}$, the acceleration vector due to global rotational movement of the segment, $\hat{a}_{O \text{ SEGi}}$, the acceleration vector due to local rotational movement of the segment, $\hat{a}_{C \text{ SEGi}}$, and the acceleration vector due to gravity, \hat{g} . Global rotational activity in this instance is rotational activity experienced by both segments while local rotational activity is rotational activity experienced by an individual segment.

$$\hat{a}_{T \text{ SEGi}} = \hat{a}_{L \text{ SEGi}} + \hat{a}_{O \text{ SEGi}} + \hat{a}_{C \text{ SEGi}} + \hat{g}. \quad (11)$$

AARMs placed on the foot and leg can be assumed to experience the same acceleration due to linear movement, global rotational movement and gravity.

Under local rotationally quasi-static conditions (i.e. whereby little or no individual segment rotational activity is occurring) $\hat{a}_{C \text{ SEGi}}$ is negligible or equal to zero and so the measured acceleration is given as

$$\hat{a}_{T \text{ SEGi}} = \hat{a}_{L \text{ SEGi}} + \hat{a}_{O \text{ SEGi}} + \hat{g}. \quad (12)$$

In this case the total acceleration vector measured by each sensor unit is a different measurement of the same vector, $\hat{a}_{T \text{ SEGi}}$, and the acceleration vector can thus be used as common vector number two.

$$\text{SENi} \hat{v}_{2(k)} = \text{SENi} \hat{a}_{T \text{ SEGi}}. \quad (13)$$

When local rotational activity of a segment occurs, the total acceleration vector will include a significant local rotational acceleration component and the sensor units will no longer measure a common acceleration vector. During such periods the second common vector can be obtained by rotational mapping of the most recent common acceleration vector using the equation.

$$\text{SENi}^{(k)} \hat{v}_2 = \text{SENi}^{(k)} \hat{a}_{T \text{ SEGi}(p)} = \text{SENi}^{(k)} R_{\text{SENi}(p)} \text{SENi}^{(p)} \hat{a}_{T \text{ SEGi}(p)}. \quad (14)$$

$\text{SENi}^{(p)} \hat{a}_{T \text{ SEGi}(p)}$ is the most recent common acceleration vector described with respect to the sensor coordinate system at the instant p it occurred $\text{SENi}^{(k)} R_{\text{SENi}(p)}$ is the rotation matrix used for the rotational mapping and it describes the orientation of the sensor coordinate system at sample point p with respect to the orientation of the sensor coordinate system at the current sample point k . $\text{SENi}^{(k)} R_{\text{SENi}(p)}$ is obtained using Eq. (15) where A is a 3×3 matrix calculated from strapdown integration of the rate gyroscope signals (Titterton and Weston, 2004).

$$\text{SENi}^{(k)} R_{\text{SENi}(p)} = \text{SENi}^{(k-1)} R_{\text{SENi}(p)} A_{(k-1)}. \quad (15)$$

The accuracy of the mapped acceleration vector as the second common vector is limited in time due to errors caused by integration drift in the strapdown integration of the gyroscope signals. Periodic occurrences of local rotationally quasi-static conditions are thus required to reset the common acceleration vector.

Algorithm 2 is used to distinguish between periods of local rotational dynamic and local rotational static activity ($N = 0.2f_s$ samples). If the local rotational activity of the segments is static then the magnitude of the acceleration vector at each sensor unit will be approximately equal (the difference is less than the pre-defined scalar threshold β). Also the angular velocity of each segment about each axis of the reference coordinate system will be approximately equal (the difference is less than the pre-defined 3×1 vector threshold $\hat{\alpha}$). If these requirements are not met then the local rotational activity of the segments may be considered to be dynamic.

Algorithm 2.

```

If
   $\frac{1}{N} \sum_{k=N}^k \left| \left| \text{SENi}^{(k)} \hat{a}_{T \text{ SEGi}(k)} \right| - \left| \text{SENi}^{(k)} \hat{a}_{T \text{ SEGi}(k)} \right| \right| < \beta$ 
AND
   $\frac{1}{N} \sum_{k=N}^k \left( \text{REF}^{(k)} \hat{\omega}_{\text{SEGi}(k)} - \text{REF}^{(k)} \hat{\omega}_{\text{SEGi}(k)} \right) < \hat{\alpha}$ 
then
  (local rotational activity is static)
else
  (local rotational activity is dynamic),
  
```

where $\text{REF}^{(k)} \hat{\omega}_{\text{SEGi}(k)} = \text{REF}^{(k)} \bar{R}_{\text{SENi}(k)} \cdot \text{SENi}^{(k)} \hat{\omega}_{\text{SEGi}(k)}$ is an estimate for the angular velocity of each segment with respect to the reference coordinate system. It is only an estimate because there will be a very slight difference between the reference coordinate system observed by the two sensor units

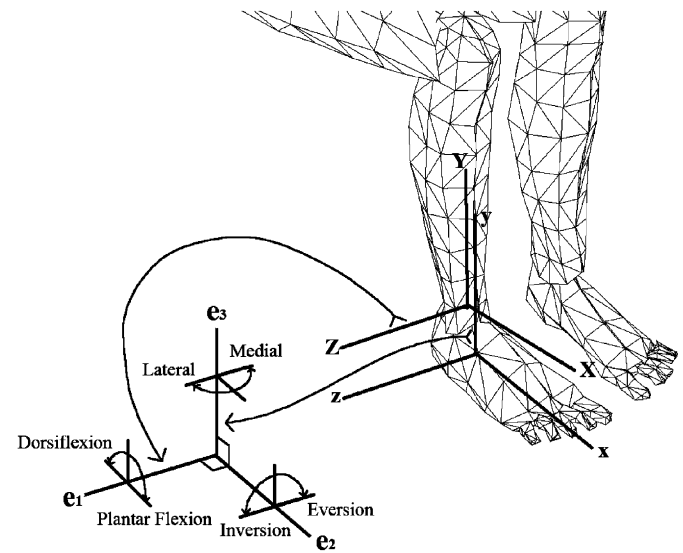


Fig. 2. Axis definitions for the derivation of the ankle Joint Coordinate System.

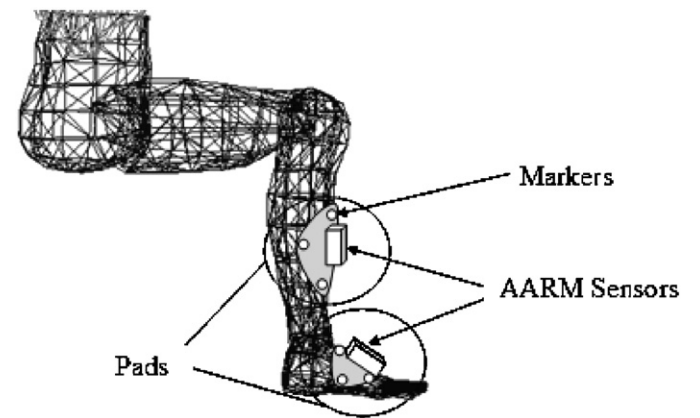


Fig. 3. Experimental set-up showing AARM sensor and Evart motion analysis marker placement for the evaluation of the proposed technique for joint angle measurement.

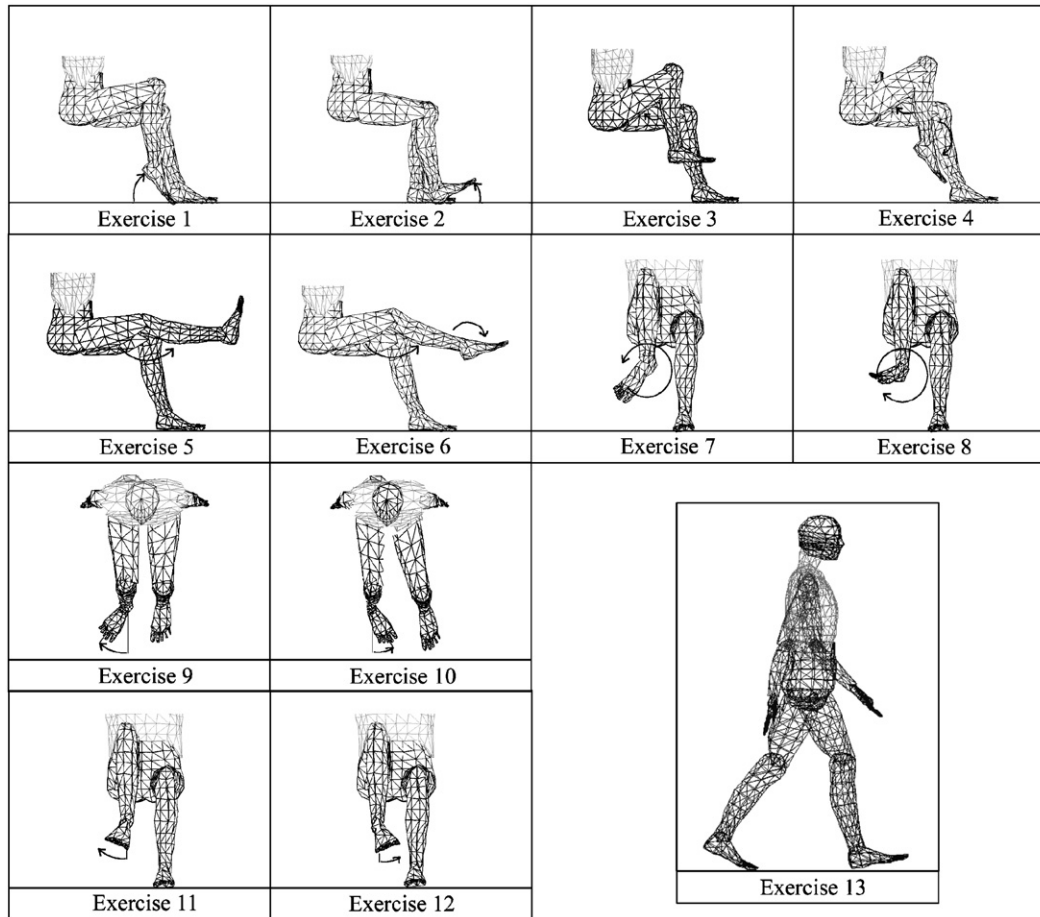


Fig. 4. Exercises performed during the evaluation of the proposed technique for joint angle measurement.

as the acceleration due to local rotational activity begins to become a significant component of the total acceleration vector. This estimate is sufficiently accurate for the process for which it is required.

2.6. Joint Coordinate System (JCS)

The three different angles of rotation at the ankle joint (dorsiflexion/plantar flexion, internal/external rotation and inversion/eversion) are calculated using a JCS (Grood and Suntay, 1983; Wu et al., 2002) obtained from the ${}^{\text{REF}(k)}\mathbf{R}_{\text{SEG1}(k)}$ and ${}^{\text{REF}(k)}\mathbf{R}_{\text{SEG2}(k)}$ derived in Section 2.4. The JCS with unit coordinate vectors \hat{e}_1 , \hat{e}_2 and \hat{e}_3 is formed by selecting \hat{e}_1 to coincide with the z-axis of the lower leg, \hat{e}_3 to coincide with the y-axis of the foot and the floating axis \hat{e}_2 the common axis perpendicular to \hat{e}_1 and \hat{e}_3 (see Fig. 2).

3. Evaluation

3.1. Experiment

An experimental trial was designed to evaluate the joint angle measurement technique. Due to ethical approval limitations the investigation of the performance of the technique in this study was limited to a static system (no accelerations except those caused by gravity and body movements existed). Ethical approval was obtained for the

experiment from the University of Limerick Research Ethics Committee. Two healthy male subjects aged 25 and 23 were recruited and informed consent was obtained from each subject. The joint angle measurement technique was tested by comparison with the laboratory based Evart¹ 3D motion analysis system. Two identical AARMS were built housing the required sensors in a plastic casing of dimensions 60 mm × 40 mm × 24 mm. A modified shin pad was attached at the front of the lower leg and a second pad was attached to the superior surface of the foot as in Fig. 3. Three markers and a single AARM sensor unit were attached to each pad.

The orientation matrix describing the orientation of the marker frame with respect to the segment frame was calculated using a technique identical to that described in Section 2.3. The sensor signals were low-pass filtered with a cut-off frequency of 15 Hz and recorded through analogue inputs in the motion analysis system with a sampling frequency of 500 Hz. The marker data was recorded at 100 Hz.

¹Motion Analysis Corporation, 3617 Westwind Boulevard, Santa Rosa, CA 95403, USA.

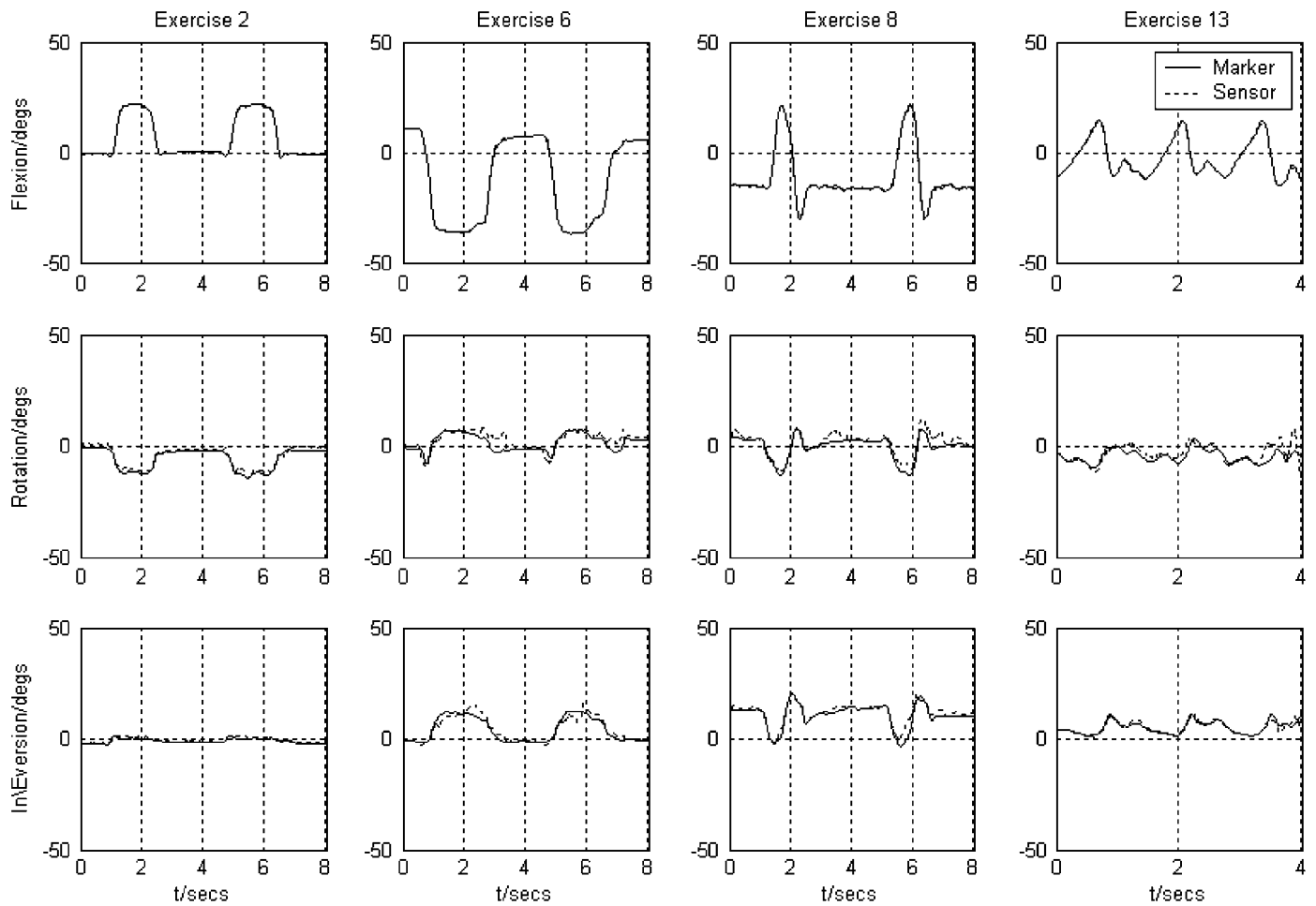


Fig. 5. Comparison of ankle joint angle data obtained from the Evart motion analysis system and the AARM sensor system. Sample data is shown for all three angles for exercises 2, 6, 8 and 13 from subject 2. Two repetitions over 8 s of all exercises are shown except for exercise 13 (ambulation) which shows a 4 s sample of three strides.

Each subject was asked to perform each of the 13 leg exercises outlined in Fig. 4. Seated exercises were performed for 10 repetitions using the right leg only. The 13 exercises investigated were:

1. Heel rise foot pumps
2. Toe rise foot pumps
3. Knee flexion with minimal foot movement
4. Knee flexion with plantar flexion
5. Knee extension with minimal foot movement
6. Knee extension with plantar flexion
7. Clockwise ankle rotation
8. Anti-clockwise ankle rotation
9. Lateral foot rotation
10. Medial foot rotation
11. Eversion
12. Inversion
13. Ambulation

The exercises were chosen to cover a wide spectrum of 3D lower leg movements. While the number of subjects

used was limited to two, the range of movement over which the technique was evaluated was large and comprehensive.

3.2. Analysis

The MATLAB² computing program was used for all post-trial data processing and analysis. Both the sensor and marker data were low-pass filtered at 5 Hz using a second order Butterworth filter. Joint angle measurements were calculated based on the JCS methods described in Section 2.6.

The root mean squared error (RMSE) of the angles measured by the sensor-based system when compared with the angles measured by the Evart motion analysis system was used to compare the two methods. The RMSE was calculated as shown below, where A represents the angle being measured (flexion, internal/external rotation or in/eversion), S represents that measured using the AARM sensor technique and E represents that measured

²The MathWorks Inc., 3 Apple Hill Drive, Natick, MA 01760-2098, USA.

using the Evart system:

$$RMSE_A = \sqrt{\frac{1}{T} \sum_{k=1}^T (\phi(k)_A^S - \phi(k)_A^E)^2} \quad (16)$$

4. Results

Fig. 5 shows a comparison of ankle joint angle data calculated using the Evart motion analysis system with that calculated using the AARM sensor technique. Sample data is shown for all three angles for exercises 2, 6, 8 and 13 from subject 2. Two repetitions over 8 s of all exercises are shown except for exercise 13 (ambulation) which shows a 4 s sample of three strides.

Fig. 6 shows a box plot of the RMSEs in degrees of the angles measured using the AARM sensor-based technique when compared with the angles measured by the Evart motion analysis system for each of the three angles of the JCS for both subjects. The horizontal lines illustrate median values, inter-quartile ranges (IQR) are illustrated by the upper and lower limits of the boxes, full ranges are

illustrated by the upper and lower limits of the vertical lines and the '+' signs illustrate outliers.

5. Discussion

5.1. Accuracy of kinematic measurements

The sample data presented in Fig. 5 shows a strong correlation between the joint angles measured using the AARM sensor based technique and the Evart motion analysis system. The experimental results presented in Fig. 6 provide an overview of the overall performance of the technique. The consistency of the performance level of the technique may be observed in this figure.

Angular errors given in degrees were smallest for the angle of flexion (subject 1 median = 0.55, IQR = 0.3, subject 2 median = 0.43, IQR = 0.48) and largest for the angle of internal/external rotation (subject 1 median = 4.09, IQR = 2.35, subject 2 median = 2.57, IQR = 1.1) for both subjects.

The superior performance of the technique in the measurement of angle of flexion may be explained by considering the derivation of the reference coordinate system from the two reference vectors (Section 2.4). In this

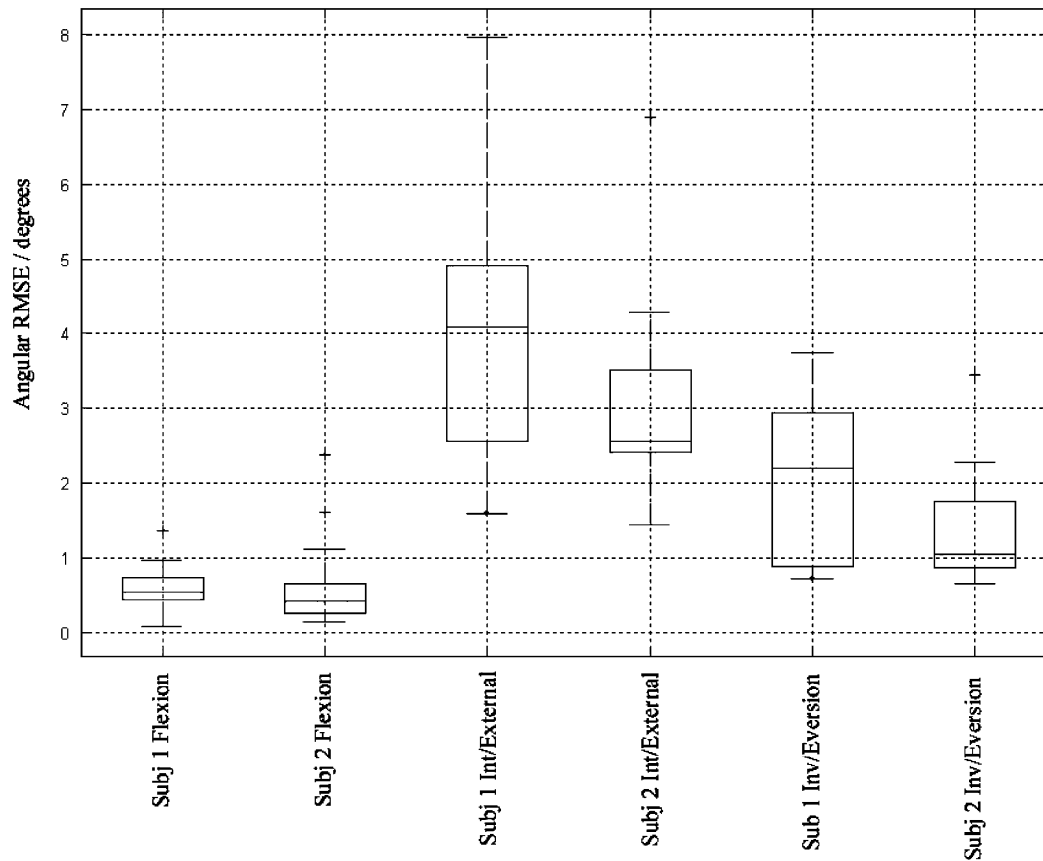


Fig. 6. Box plot of the RMSEs in degrees of the angles measured by the sensor-based system when compared with the angles measured by the Evart motion analysis system for each of the three angles of the Joint Coordinate System for both subjects. The horizontal lines illustrate median values, inter-quartile ranges (IQR) are illustrated by the upper and lower limits of the boxes, full ranges are illustrated by the upper and lower limits of the vertical lines and the '+' signs illustrate outliers.

experiment the acceleration reference vector was generally the gravity vector (no global rotational or linear acceleration existed). The magnetic inclination in Limerick, Ireland is approximately 67° and so the angle between the two reference vectors is approximately 23° as opposed to being ideally orthogonal. The joint angle measurement technique was thus more sensitive to rotations about the axis orthogonal to the two reference vectors, ${}^{\text{SENi}(k)}\hat{x}_{\text{REF}(k)}$, than it was to rotations about either of the reference vectors themselves. In this experiment flexion rotations were generally performed about an axis approximately orthogonal to the two reference vector, thus resulting in the most accurate measurements. Internal/external rotations were generally performed about the acceleration reference vector, thus resulting in the least accurate measurements. Inversion/eversion rotations were generally performed about an axis which was neither a reference vector nor an axis approximately orthogonal to the two reference vectors and the accuracy of the measurement of these rotations reflected this, lying approximately in between the accuracy of the other two.

5.2. Contributions of this study and future work

This study has outlined a technique for 3D inter-segment ankle-joint angle measurement. The technique may be suitable for use in a dynamic system such as a moving vehicle. The investigation of the performance of the technique in this study was limited to a static system. A future study should seek to investigate the performance of the technique in a dynamic system.

Acknowledgement

The authors would like to thank the Irish Research Council for Science, Engineering and Technology for their sponsorship of this project.

Appendix A. Supplementary materials

Supplementary data associated with this article can be found in the online version at [doi:10.1016/j.jbiomech.2006.12.010](https://doi.org/10.1016/j.jbiomech.2006.12.010).

References

Bachmann, E.B., 2000. Inertial and magnetic tracking of limb segment orientation for inserting humans into synthetic environments. Ph.D. Thesis, Naval Postgraduate School, Monterey, CA, p. 178.

- de Vries, W., Veltink, P.H., Koper, M.P., Koopman, B.F.J.M., 1994. Calculation of segment and joint angles of the lower extremities during gait using accelerometers. In: Proceedings of the Second World Congress of Biomechanics on Dynamic Analysis Using Body Fixed Sensors, McRoberts, Amsterdam.
- Ferraris, F., Grimaldi, U., Parvis, M., 1995. Procedure for effortless in-field calibration of three-axis rate gyros and accelerometers. *Sensory Materials* 7, 311–330.
- Foxlin, E., 1996. Inertial head-tracker sensor fusion by a complementary separate-bias Kalman filter. In: Proceedings of the IEEE Virtual Reality Annual International Symposium, 1996, Santa Clara, CA.
- Good, E.S., Suntay, W.J., 1983. A joint coordinate system for the clinical description of three-dimensional motions: application to the knee. *Journal of Biomechanical Engineering* 105, 136–144.
- Kemp, B., Janssen, A.J., van der Kamp, B., 1998. Body position can be monitored in 3D using miniature accelerometers and earth-magnetic field sensors. *Electroencephalogr Clin Neurophysiol* 109, 484–488.
- Lötters, J.C., Schipper, J., Veltink, P.H., Olthuis, W., et al., 1999. Procedure for in-use calibration of triaxial accelerometers in medical applications. *Sensors and Actuators* 68, 221–228.
- Luinge, H.J., Veltink, P.H., 2005. Measuring orientation of human body segments using miniature gyroscopes and accelerometers. *Medical and Biological Engineering and Computing* 43, 273–282.
- Lyons, G.M., Culhane, K.M., Hilton, D., Grace, P.A., et al., 2005. A description of an accelerometer-based mobility monitoring technique. *Medical Engineering and Physics* 27, 497–504.
- Mayagoitia, R.E., Nene, A.V., Veltink, P.H., 2002. Accelerometer and rate gyroscope measurement of kinematics: an inexpensive alternative to optical motion analysis systems. *Journal of Biomechanics* 35, 537–542.
- Roetenberg, D., Luinge, H.J., Baten, C.T., Veltink, P.H., 2005. Compensation of magnetic disturbances improves inertial and magnetic sensing of human body segment orientation. *IEEE Transactions on Neural Systems and Rehabilitation Engineering* 13, 395–405.
- Rukstales, K.S., Quinn, J.M., 2001. Inclination chart, the international geomagnetic reference field, 2000. In: Geologic Investigations Series I-2754, International Association of Geomagnetism and Aeronomy.
- Titterton, D.H., Weston, J.L., 2004. Strapdown navigation system computation. In: Strapdown Inertial Navigation Technology, Institution of Electrical Engineers, Hertfordshire, pp. 309–313.
- Veltink, P.H., Slycke, P., Hemssems, J., Buschman, R., et al., 2003. Three dimensional inertial sensing of foot movements for automatic tuning of a two-channel implantable drop-foot stimulator. *Medical Engineering and Physics* 25, 21–28.
- Williamson, R., Andrews, B.J., 2001. Detecting absolute human knee angle and angular velocity using accelerometers and rate gyroscopes. *Medical and Biological Engineering and Computing* 39, 294–302.
- Willemsen, A.T., van Alste, J.A., Boom, H.B., 1990. Real-time gait assessment utilizing a new way of accelerometry. *Journal of Biomechanics* 23, 859–863.
- Wu, G., Siegler, S., Allard, P., Kirtley, C., et al., 2002. ISB recommendation on definitions of joint coordinate system of various joints for the reporting of human joint motion—part I: ankle, hip, and spine. *Journal of Biomechanics* 35, 543–548.